UNIVERSITY OF CALIFORNIA, LOS ANGELES
DEPARTMENT OF MECHANICAL, AEROSPACE AND NUCLEAR ENGINEERING

NASA/USRA ADVANCED DESIGN PROGRAM
1990-91

JULY 10, 1991

University of California, Los Angeles

Department of Mechanical, Aerospace, and Nuclear Engineering

MANNED VOYAGE TO MARS, WITH PERIODIC REFUELING FROM ELECTRICALLY PROPELLED TANKERS

ABSTRACT

Twenty-four UCLA students, in groups of four or five participated in a mission design for a manned expedition to Mars that was based on the concept of mid-course refueling from electrically propelled tankers launched ahead of the manned mission. This study was conducted during the 1991 spring term.

Some of the student groups opted for non-nuclear propulsion of the manned ship, based on LOX and LH2, others opted for one based on nuclear-thermal propulsion. By way of example, the first option is presented below.

1. INTRODUCTION

Electric thrusters, such as the already well developed ion engines of the electron bombardment type, can have a very large specific impulse, but for realistic levels of electric power, have low thrust, resulting in very long travel times. In this mission analysis, it is proposed to combine their advantage (high Isp) with the advantage of chemical propulsion (high thrust) by mid-course refueling the chemically propelled, manned ship by means of electrically propelled, unmanned tankers. This option therefore represents a non-nuclear alternative to the nuclear-thermal option recommended by the Augustine Committee.

The tankers, which will be orbiting for periods of 3 to 8 years, will be launched a corresponding number of years before the start of the manned ship. In addition to their own propellant (liquid argon), the tankers carry a much larger quantity of LOX and LH2 for transfer to the manned ship. In the present study, the tankers' electric power is provided by a 2 to 5 megawatt (electric) type nuclear reactor, with, for instance, a potassium Rankine cycle power converter. Boiloff of the cryogenic propellants is recondensed by sorbent pumps using the reactor's waste heat.

Refueling the manned ship n times is equivalent to an $(n + 1)$ fold increase in Isp.

Because of the very high Isp of the tankers, the total mass that must be assembled in LEO is greatly reduced.

A second feature that may be applied to such a mission is to produce all the LOX, even the one for the initial fueling, either from lunar soil or, alternatively, from the Martian atmosphere. In the latter case, the tankers would start from LEO only with hydrogen, land on Mars, autonomously manufacture the LOX, go into a low altitude orbit about Mars by expending a relatively minor amount of LOX and LH2, and return to LEO (or to orbital matching for a mid-course rendez-vous with the manned ship). The advantage here derives from the fact that the difference in total energy (gravitational plus kinetic) per unit mass is 3.3×10^7 m^2/s^2 for ascending from the ground to LEO (assumed here, and in what follows, at the Space Station Freedom altitude) vs. only 6.6×10^6 m^2/s^2 for the ascent from the Mars surface to a low Mars orbit (assumed at 200 km altitude). Because of the high Isp of the tankers, the transport from Mars vicinity to Earth vicinity is sufficiently efficient in propellant usage so as to reduce by a major factor the total mass that must be brought up to LEO.

Ordinarily, low thrust, electrically propelled spacecraft are intended to apply thrust parallel to the instantaneous flight path. This then results in a spiral path, nearly circular at all times, about the astronomical body. However, such a path will not allow rendez-vous with a manned ship that is on an efficient, short travel time trajectory. It is then advantageous to put the entire burden for the needed matching of position and velocity on the tankers. This can only be accomplished by applying thrust at an angle to the tankers' flight path (except at the periapsis where the angle is zero). For the trajectories of interest, it can be shown that, as a consequence of thrusting obliquely to the flight path, roughly 1/2 of the delta V is lost by not contributing to an increase in total energy.

2. TRAJECTORY ANALYSIS

The refueling craft (tankers) employ ion-engines with very large specific impulse but very low thrust. These craft are in orbit for 3 to 8 years prior to the launch of the manned ship and carry the necessary fuel for them.

In order to achieve the most efficient path for the ion-tankers, a spiral path with a

2

thrust parallel to the instantaneous flight path would have to be followed, but such a trajectory would not allow the manned ship to rendezvous with the tanker. The matching of the position and the velocity must be achieved by applying thrust at an angle to the flight path so as to produce an elliptic orbit coincident with the manned ship orbit. This study will look into the concept of a low-thrust, constant-periapsis-radius trajectory for the ion-tankers. It is important to note that such a trajectory is not optimal in terms of time and propellant use, but will be used here to study the overall feasibility of the mission.

2.1 Manned Ship Trajectory: From the manned ship trajectory, the velocities were calculated for both transfer ellipses. The results for the transfer to Mars produced ΔV's for different injection points from launches at 186.9° to 336.9° true anomaly in the Mars reference frame in increments of 10°. The semi-major axis lengths were chosen from 2 to 8 A.U. at increments of 1 A.U.

The results showed that as the semi-major axis length approached the minimum energy semi-major axis length, the ΔV requirements became smaller. However, if such a semi-major axis length was chosen for the first leg of the mission, then the ΔV's for the return trip to Earth became unacceptably high. A compromise had to be made between the requirements for the first and second leg of the manned mission.

A transfer ellipse defined by a launch true anomaly of 276.9° and a semi-major axis length of 2 A.U. was chosen. The point of injection and the transfer ellipse are not optimal, but were chosen because they produced acceptable ΔV's for the return trip.

The velocities in the Earth, Sun and Mars frames of reference, the refueling points, and the elapsed mission times in sidereal days are indicated in Figures 1 and 2.

2.2 Trajectories of the Ion Engine Propelled Tankers: This part of the study was designed to investigate the use of ion-engine-propelled craft for the purpose of refueling and preboosting supplies and equipment to Mars. For the proposed mission, refueling craft are stationed in a highly elliptical orbit about Earth, similarly about Mars, and finally in an orbit about the Sun. The orbit about the Sun is necessary in order for a rendezvous to be
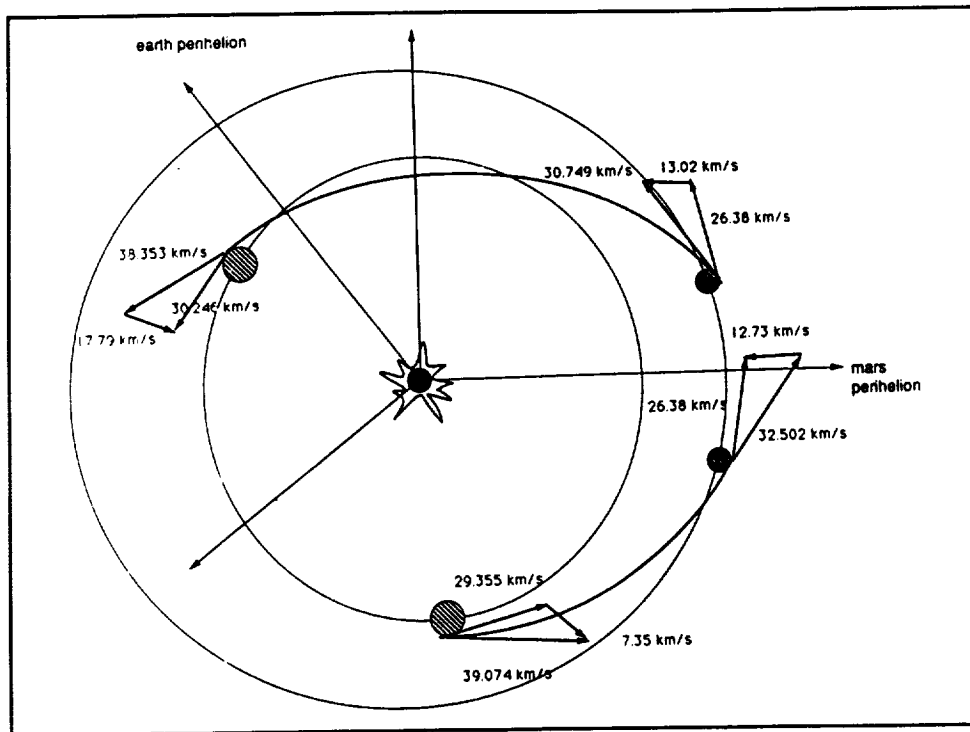
Figure 1: Manned Ship Velocities in the Earth, Sun and Mars Reference Frames
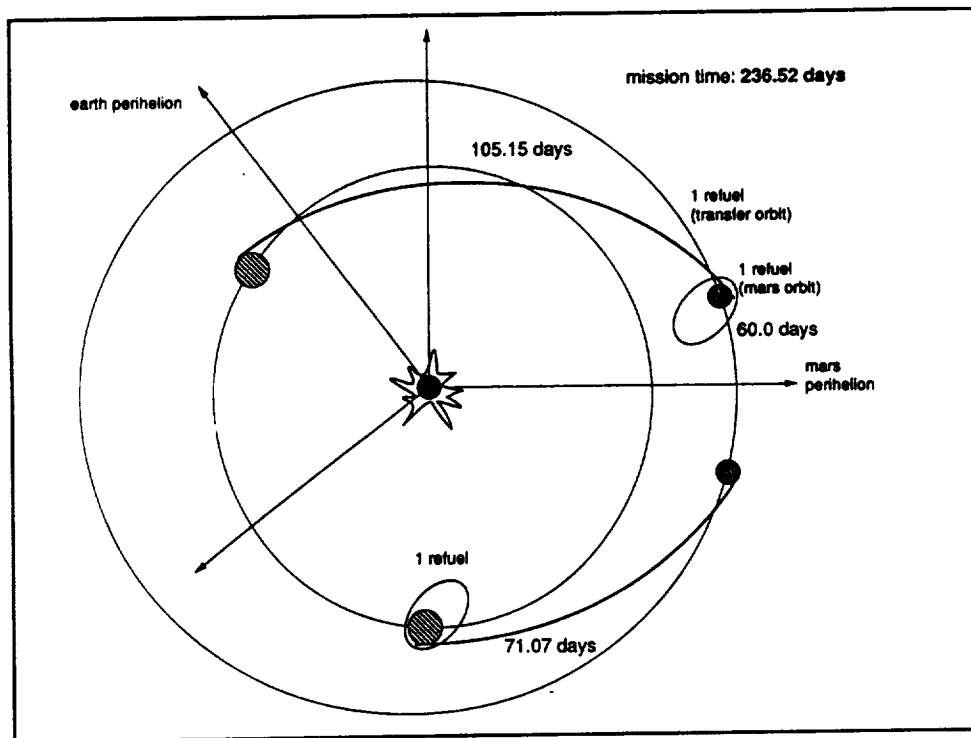
Figure 2: Refueling Points (Rendez-Vous with Tankers) and Elapsed Days for the Manned Mission

4

achieved after a hyperbolic escape from Mars. Each set of refueling craft carries the necessary fuel to complete its leg of the trip. The masses of fuel were calculated by the velocity requirements for each stage of the mission.

It was calculated that for a manned ship with a mass of 58 metric tons the fuel needed would require 2 tankers with masses of 691,000 kg for the boost back from Mars. One of these tankers would rendezvous with the manned ship in an elliptic orbit about Mars, and the other would rendezvous after the hyperbolic escape. For the boost from Earth, only one tanker ship would be required.

Several parameters were specified:

initial mass m_o = 691,167 kg

I_{sp} = 10,000 s

thrust = 50 N

For the first refueling ship, the escape from Earth required approximately 4.47 years. For the second refueling ship, some difficulties were experienced due to the high sensitivity of the program to several parameters. In the transfer phase, by altering the parameter, the transfer time and the number of revolutions around the Sun were altered significantly. For the transfer from Earth to Mars, further investigation is necessary for a more efficient transfer, using trajectories without maintaining a constant periapsis radius. Such a trajectory is more appropriate for tankers being sent to Mars, so as to reduce the transfer time and the fuel for the ship. Figure 3 shows computed trajectories for the first tanker, leading up to Earth escape. The parameter k associated with each orbit indicates its approximate multiplicity. For instance, the innermost orbit with k = 1651 indicates that roughly the same orbit is travelled 1651 times before reaching the next higher orbit. This method of approximation, although crude compared with averaging methods such as the Krylov-Bogoliubov method, proved to be adequate for our purposes.

Maintaining a constant perigee radius of the tanker orbits is necessary for matching the manned ship velocity at the refueling points. To accomplish this, the direction of the thrust (assumed to be of constant magnitude) must vary along the orbit. Figure 4 shows the result of the computer program that was developed to calculate the angle α between the thrust and the tangent to the orbit.

5

For a configuration of
Isp=10,000 s
Thrust=50 N
Mo=.69e6 kg

Final orbit:

i=10/k=140

θ=166° -> ρ=71.10

gives

Ttotal=4.42 years

i=9/ k= 289
a=9.92 ro

i=8/ k=444
a=4.99 ro

i=7/ k= 620
a=3.33 ro

i=4/ k= 1154
a=1.67 ro

i=2/ k= 1651
a=1.25 ro
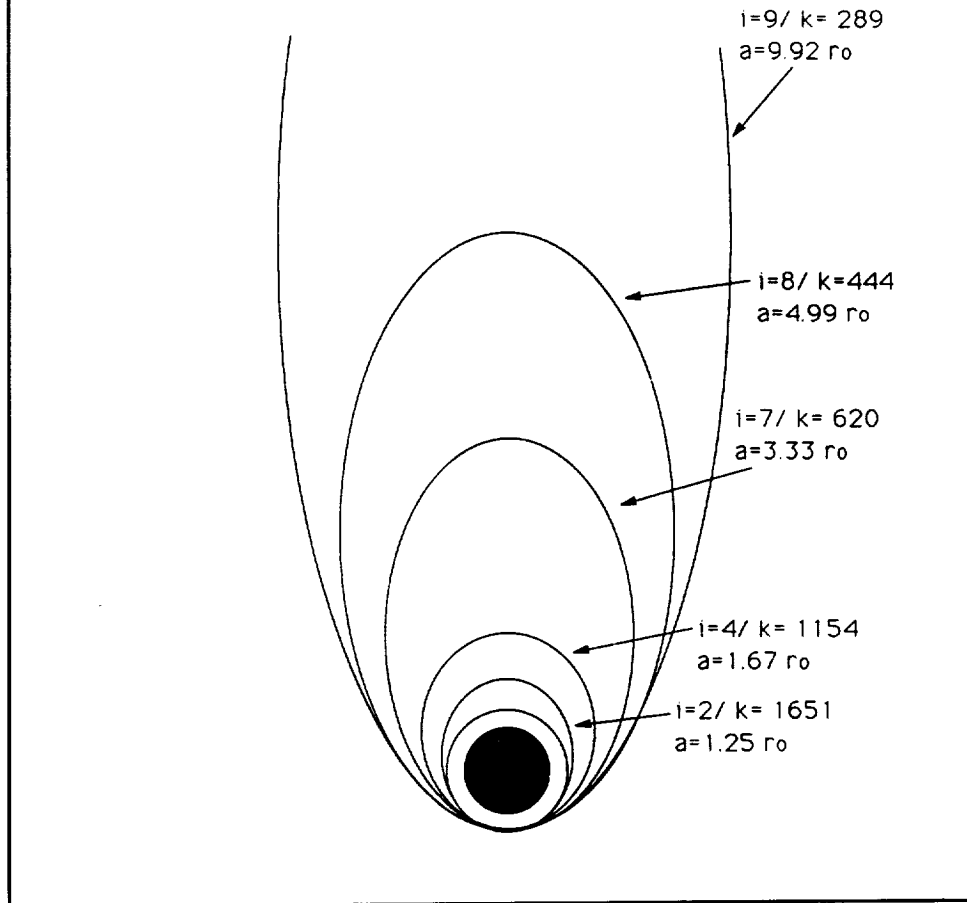
Figure 3: Earth Escape of Ion-Engine Propelled Tanker (Each Ellipse Represents a Large Multiplicity of Roughly Equal Orbits)
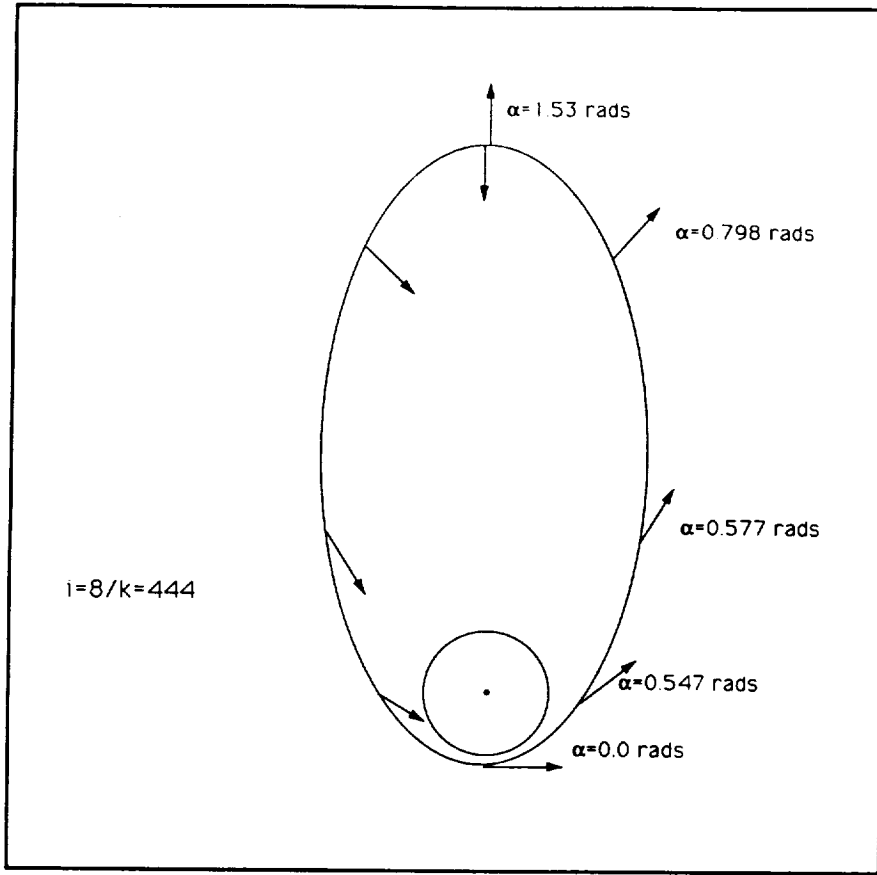
Figure 4: Computed Direction of the Thrust Needed to Result in a Sequence of Orbits with Constant Periapsis Radius

2.3 Mars and Earth Aerobraking: The velocity of the manned ship approaching Mars has a relative velocity of 13.63 km/s. A retro-fire of 6.49 km/s is made to slow the ship to 7.13 km/s in which the manned craft will enter the atmosphere at a r_p of 3446 km. After the craft has left the atmosphere, an orbit with the following parameters is established.

$$e \quad = 0.998$$

$$a \quad = 19919 \text{ km}$$

$$r_p \quad = 3446 \text{ km}$$

Another burn is then made to increase the periapsis to match the Mars parking orbit.

$$\Delta V \quad = 0.02591 \text{ km/s}$$

$$e \quad = 0.975$$

$$a = 20145 \text{ km}$$
$$r_p = 3898 \text{ km}$$
$$V_p = 4.41 \text{ km/s}$$
$$T = 2\pi(a^3/\mu)^{1/2} \text{ (sec)}$$
$$= 24.641 \text{ hrs}$$

Once this orbit is established, a rendezvous is made with the ion-tanker for refueling. Figures 5 and 6 show schematically these phases of the manned ship trajectories.
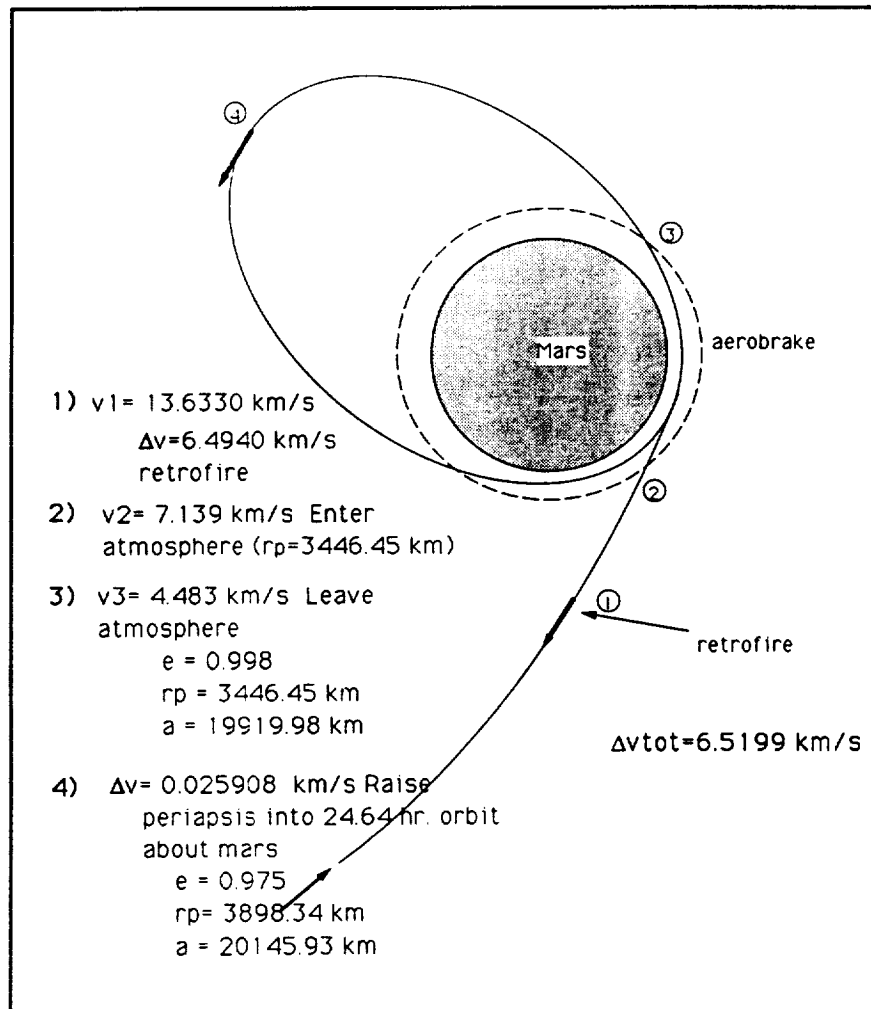
Figure 5: Mars Injection
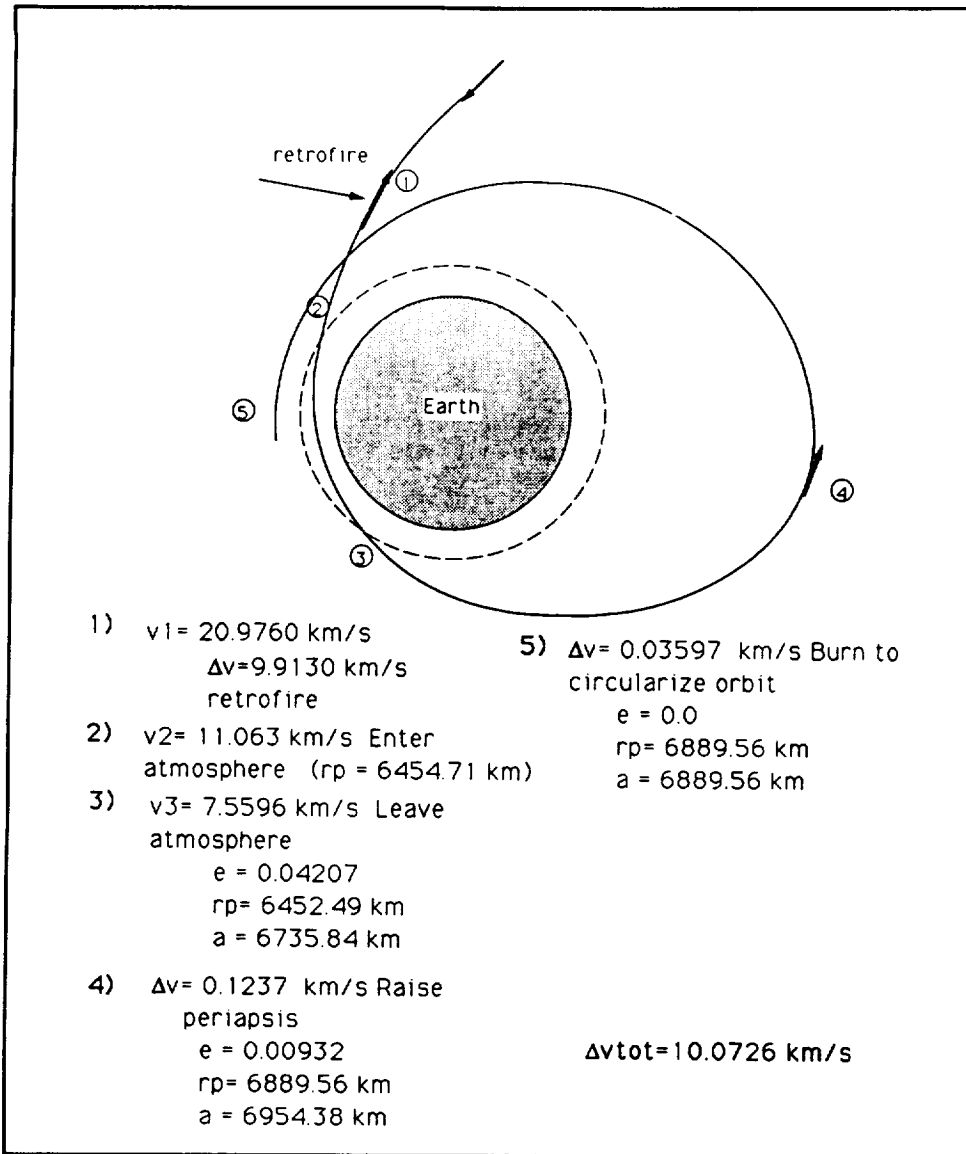
Figure 6: Aerobraking Preceding Return to Earth

3. THERMAL SUBSYSTEMS

3.1 Tanker Ship Power Cycle Analysis: The power requirements for the ion-engine propelled tankers are shown in Table 1. Each ion engine was assumed to develop a thrust of 2 N with a power requirement of 91.96 kWe. The total engine requirements are then calculated using the ion tanker thrust requirement of 50 N and 5 extra engines for reliability. This results in a total engine requirement of 2.7 MWe.

9

Ion Tanker Thrust Requirement (N)	50
Number Thrusters (5 Redundancy)	30
ARGON Thrusters:	
Isp (s)	10,000
Thrust (N)	2
Electric Power (kWe)	91.9
Mass (kg)	100
Total Power Required (MWe)	3.3
Potassium RANKINE Cycle Requirements:	
Power Cycle Efficiency	0.12
Total Reactor Power Required (MWt)	27.5
Cycle Starting Points:	
Qth input (MW)	27.5
Qth output (MW)	24.2
Total Mass (kg)	3000
Total Thrust Available (N)	60
Power Required (MWe)	2.75
System Additions (MWe):	0.54
Cryogenics	
Instruments, Housekeeping	

Table 1: Ion Engine Requirements and System Configuration

The author of Ref. 4 discusses the viability of closed Brayton cycle power conversion with the SP-100 reactor, which provides 0.1 MWe, and shows that the Brayton cycle has advantages over thermoelectric technology, especially in cycle efficiency that leads to a decrease in reactor and shield masses, a smaller thermal heat output and smaller radiator areas.

In Ref. 1, various Brayton and Rankine cycle configurations are compared with a variety of working fluids for a Pellet Bed Reactor power conversion for Strategic Defense Initiative use. The system chosen with the lowest ratio of electric power to mass is a double loop cycle consisting of a primary H_2 reactor cooling loop, connected to a potassium Rankine cycle through a counter-flow heat exchanger. This system can provide 3.3 MWe during alert modes of operation, or 165 MWe of electric power during brief burst modes of operations. The primary reactor cooling loop is constrained to operate at 12 MPa, while the

secondary potassium loop operates at 0.84 MPa during the alert mode. The Rankine cycle has been modified with the reheater and low pressure turbine to increase efficiency. Although the Rankine cycle reaches an efficiency of 20.3%, the losses incurred in the primary cooling loop and the heat exchanger give an overall plant efficiency of 12.0%. This translates to a reactor thermal output of 28 MWth. At these power rates, the power conversion cycle must reject 24.7 MWth through the radiator, which operates at an average temperature of 1,116 K. On the one hand, a high rejection temperature decreases the overall efficiency of the system, requiring more thermal input power. On the other hand, a high radiator rejection temperature, ensures a low radiator weight, as will be discussed below.

A low temperature heat transfer loop is required to transport heat away from the alternator, generator, ion drives, and electronics. Reference 15 estimates the requirements for an ion propelled nuclear vehicle to be 150 KWth dissipated at 373 K. For this type of application, the authors suggest a helium cooling loop with an auxiliary radiator loop.

This power system can accommodate the needs of the Mars mission tankers, providing an additional 541 kWe for any necessary housekeeping functions, communications, and cryogenic cooling. The energy requirements of the tankers are 2.2% of the burst mode capabilities of the Pellet Bed Reactor. The system mass quoted in Ref. 1 reflects the power load incurred by the burst energy requirements. Therefore, an effort was undertaken to review the current literature to find size reductions for each individual power cycle component.

3.2 Boiler and Reheater Design: Reference 1 shows a preliminary design for the boiler/superheater and the reheater. Both use a counter-flow configuration to increase the heat transfer rate. Thin twisted ribbons in the boiler tubes produce a small centrifugal force that provides for two-phase separation. The heat exchanger designed for the burst option of Ref. 1 has a mass of 11,000 kg and a boiler and reheater inlet temperature of 2,196 K and 2,278 K, respectively. The corresponding H_2 reduced temperatures for the alert mode of operation are 1,816 K and 1,808 K, showing that some reduction in heat exchanger mass is in order using the 3.3 MWe ceiling. The temperature reduction available in Ref. 1 for 3.3

11

MWe is about 40%. A conservative reduction in heat exchanger mass of 30% will be assumed in this report, for an overall vapor generator mass of 7,700 kg.

3.3 Turbine Design: The turbines selected for the Rankine cycle quoted in Ref. 1 are sized at a mass of 2,500 kg for each of the two turbines. Noting that these turbines are able to deliver up to 165 MWe during peak burst outputs for the Strategic Defense Initiative configurations, efforts were made to study turbine machinery sized to the 3.3 MWe power requirement of the tanker design.

The author of Ref. 2 conducted studies on various sizes of turbines operating within different power cycles and at different working fluids. This study found that turbine mass decreased significantly with increased turbine blade speed and increased outlet temperatures. Increasing these two parameters dictates the turbine disc material, as structural loads increase significantly. For the potassium Rankine cycle, the use of a nickel superalloy for the blade discs requires that the blades be cooled to 950 K, which is standard practice in the turbine industry. Table 2 shows a comparison of the two turbine designs.

	Reference 1 High Pressure Turbine	Reference 1 Low Pressure Turbine	Reference 2 Sample Design Turbine
Inlet Temperature (K)	1800	1800	1350
Outlet Temperature (K)	1476	1185	1100
Rated Power (MWe)	1.65	1.65	1.00
Inlet Pressure (MPa)	0.84	0.45	0.963 (Saturated)
Outlet Pressure (MPa)	0.45	0.12	0.08
Turbine Efficiency	0.9	0.9	0.85
Mass (kg)	2500	2500	950

Table 2: Turbine Parameter Comparison

Table 2 shows the similarity in proposed design data for the axial flow turbines. Using an outlet temperature of 1,100 K, and a turbine speed of about 10,000 rpm, the high

pressure and the low pressure turbine can be sized at a value of about 200 kg each. This provides a very large decrease in the 2,500 kg turbine mass of Ref. 1. Special note should be made that the higher working fluid temperatures and the large angular velocity and the blades will require advanced materials possessing high strength at high temperatures.

3.4 Radiator Design: Two radiator assemblies are needed for each ion-engine propelled tanker: a high temperature radiator for rejection of the reactor waste heat and a low temperature radiator for the rejection of waste heat from the alternator, the electronics/communications bus, and the ion engines. In choosing a viable design for both radiators, the primary consideration is the mass per unit area of the panels, as they are usually quite massive. Other factors of merit in a radiator design are retractable designs for minimum launch volume, resistance to micro-meteoroid impact, material structural integrity at high temperatures, material compatibility with the working fluid, and material compatibility with high altitude atmospheric species.

The radiator areas can be calculated using the heat balance at the radiator surface,

$$A - Q_{th} /(\epsilon \sigma A T^4 - \alpha I_{sun} \cos \phi)$$

in the standard notation. This equation was solved for the required radiator area for the worst condition. The solar flux vector is assumed at a worst case incidence angle and a maximum I_{sun} in the vicinity of the Earth ($\phi = 0°$, $I_{sun} = 1353$ W/m^2). Values for the emissivity and the absorptivity were taken from Ref. 7 for end-of-life coatings common on today's spacecraft ($\epsilon = 0.85$, $\alpha = 0.21$). Using the known values of the thermal load and radiator temperature from Ref. 1, the necessary high temperature radiator area is $A = 324.97$ m^2. An additional 10% is added to account for radiative form factors. Similarly, using a temperature of 350K and an output of 150 KWth, the area of the low temperature radiator is $A = 375.82$ m^2. Several alternative radiator concepts were explored. The authors of Ref. 12 examined several options for advanced radiator designs. Liquid Droplet Radiators direct small fluid droplets off a droplet generator towards a collector. This system has the advantage of a low radiator mass, which is concentrated in the fluid droplets themselves. Many disadvantages are cited, including the loss of fluid to free space in vapor and liquid

13

form, the formation of crystals at the droplet collector, and the lack of a high emissivity fluid at high temperatures. This results in droplet sheets that are too large for this mission's applications.

Moving Belt Radiators heat a wide belt as it passes over a hot rotary drum. Heat is then dissipated to space as the belt moves away from and then returns to the drum. This system has the disadvantages of poor contact conductance between the belt and the metallic drum, and the loss of high emissivity coatings at the drum due to their brittle nature. The large belts would be outside the reactor shield shadow, resulting in neutron scattering to the liquid fuel later needed on the manned ship.

Heat pipe radiators were seriously considered for use as the high temperature radiators on the tanker ships. This technology is highly developed and has been extensively tested. With the envisioned potassium Rankine cycle, the heat pipe radiator could be configured in a variety of geometries, including the telescoping of cylindrical radiator of Ref. 5 and 12 and the deployable cone configuration of Ref. 19. Both of these geometries provided excellent thermal conductances and can easily fit within one Shuttle payload bay.

Reference 5 envisions the use of SiC fiber reinforced titanium for high temperature radiator designs. This material is compatible with potassium as a working fluid and will not degrade in reaction with high altitude atmospheric species, such as that present with carbon-carbon composites (Ref. 19) and atomic oxygen. Yet even with this advanced technology, the mass of the radiator material is still quite high, projected at 4.82 kg/m^2 for the composite titanium and much higher values (15 kg/m^2) for the cone configured carbon-carbon radiator.

The design eventually chosen for this mission is the Rotating Bubble Membrane Radiator (RBMR). As shown in Fig. 7 from Ref's. 8, 9, 12, and 15 the radiator consists of a thin membrane enveloping a central vapor sprayer. The membrane rotates relative to the attachment boom as hot vapor is sprayed from the central spray nozzle. The vapor condenses as it approaches the membrane, where it is trapped and funnelled into the return pump collection trough by the centrifugal forces. A thermal electromagnetic pump forces the fluid through the return piping for eventual return to the power conversion loop.
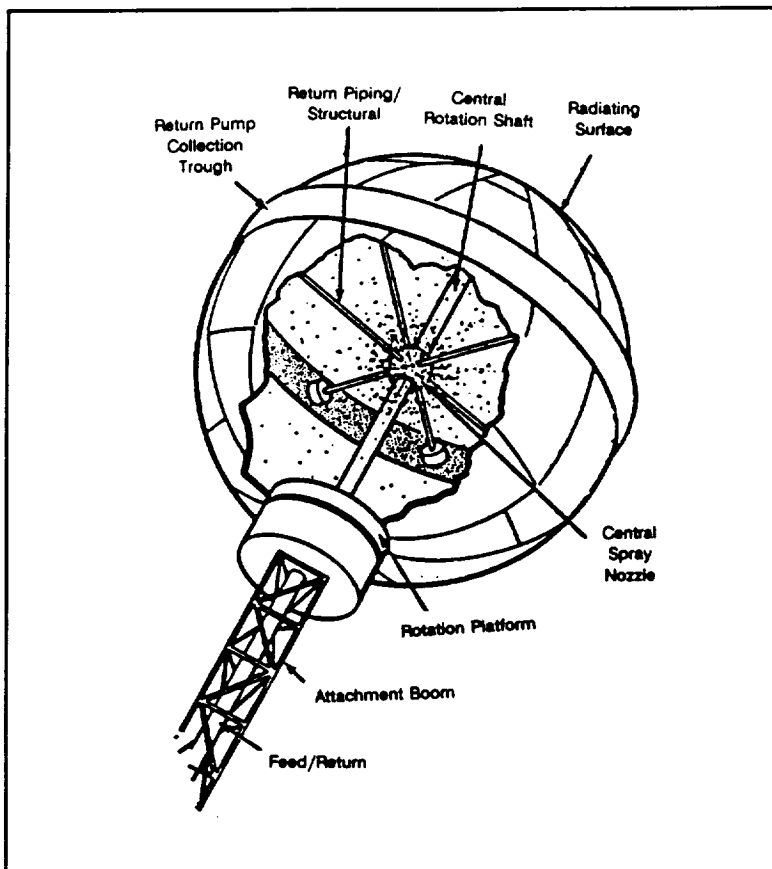
Figure 7: Boom Mounted Bubble Membrane Radiator

The RBMR has many inherent advantages. The most apparent is the low mass of the radiator compared with the heat pipe designs quoted above. For a membrane (silicon-carbide cloth with thin metallic liner) with a thickness of 0.43 mm, Ref. 8 shows a radiator mass of 1.105 kg/m^2, with an additional mass of 45.45 kg for the sprayer, pump, rotating joint, and structural tubing for each bubble. For the necessary radiator area of this mission, Table 3 shows a comparison of the different heat pipe designs and related radiator masses. Obvious mass savings are available with the RBMR.

Although the RBMR may seem highly susceptible to micrometeorite puncture due to its thin membrane skin, Ref. 8 provides convincing data showing the reliability of the radiator. Using the Near Earth to Lunar Surface Meteoroid Environmental sporadic meteoroid model developed by NASA, the authors calculated the likely number of meteoroids to collide with a radiator of 57.18 m^2 and found no major fluid loss.

15

	Reference 5	Reference 19	Reference 8
Radiator Type	SiC Reinforced Ti Telescoping Cylinder	Carbon-Carbon Composite Deployable Cone	Si-Carbide Cloth/Metallic Liner Rotating Bubble Membrane
Mass Per Area (kg/m²)	4.82	15.00	1.105 Thickness = 0.00043 m
Additional Radiator Mass (kg)	--------	--------	45.45
Radiator Area (m²)	357.47	357.47	357.47
Total Mass (kg)	1722.98	5361.98	440.45 1 Bubble, Diameter = 10.67 m
			485.90 2 Bubbles, Diameter = 7.54 m
			576.80 4 Bubbles, Diameter = 5.33 m
			758.60 8 Bubbles, Diameter = 3.77 m

Table 3: Heat Pipe and RBMR Masses

For purposes of our mission, two RMBR's were chosen for the high temperature radiator, each with a diameter of 7.54 m. This redundancy will reduce the possibility of catastrophic failure, while also reducing the radiator areas to a value more consistent with the micro-meteoroid calculations of Ref. 8. Noting that our area per radiator has increased from the 57.18 m² of the report, the reliability of our larger radiators was calculated. Reference 8 gives the corrected total meteoroid mass-flux in the near Earth orbits as

$$Log_{10}N_t = -14.37 - 1.213 \, Log_{10}m$$

where N_t = number of meteoroids of mass m or greater, per m²s

m = meteoroid mass (g)

Knowing the number of meteoroids allows the calculation of the percent of impacting meteoroids of mass m or greater, and the number of meteoroid impacts by mass group. These calculations are shown in Table 4 for the 178.733 m² radiator. Operational reliability

16

can be calculated by subtracting the percentage of all meteoroids designed against. For the 0.46 mm skin thickness calculated above, the design meteoroid mass is 0.001 g for a reliability of 0.99977.

Meteoroid Mass m (g)	Total Meteoroid Mass Flux, Nt (g/m²s)	Number Impacts of m or Greater	% Meteoroids of Mass m or Greater	Number Impacts by Mass Group
0.1	6.966E-14	0.00251	0.00009	0.00236
0.01	1.138E-12	0.04104	0.00141	0.03852
0.001	1.1858E-11	0.67017	0.02296	0.62913
0.0001	3.034E-10	10.94420	0.37497	10.27403
0.00001	4.955E-09	178.72448	6.12350	167.78028
0.000001	8.091E-08	2918.66356	100	2739.93908

Table 4: Radiator Meteoroid Impact

The use of two radiators also allows for rotation opposition, effectively eliminating any reaction torques encountered at the rotating joints (low friction BAPTA interfaces). The use of two radiators introduces a geometric form factor into the area calculation, because part of the emitted heat is incident upon the opposing radiator (as well as the rest of the spacecraft).

3.5 Estimated Mass: The mass of the power generating system of the refueling ships is summarized in Table 5.

COMPONENT	MASS (KG)
Reactor	4000
Neutron/Radiator Shield	4000
Hydrogen Compressor	667
Boiler/Reheater	7700
Turbines	400
TEM Pump	200
Primary Radiator	485.9
Secondary Radiator	500
Alternators/Electronics/ Generator (Ref. 15)	2500
Ion Engines	3000
Total	23452

Table 5: Thermal System Mass for One Tanker

4. SUMMARY

The manned mission was postulated to have a duration of less than one year, with an extended stay on Mars of sixty (60) days. From trajectory analysis and optimization, transit times are summarized as follows:

MISSION SEGMENT	TIME (DAYS)
Trans-Mars Injection	71
Mars Stay	60
Trans-Earth Injection	107
TOTAL	236

Mission time and total mass in LEO were major design factors. An increase in mission time causes significant increases in life support system mass, overall ship mass, propellant requirements, radiation hazard, and probability of psychological problems. Basic requirements such as food, water, light, and oxygen increase at roughly linear rates as trip times are increased. Overall ship mass increases as space is needed to accommodate the extra stores. To offset this increase in size, return trip provisions minus air and water supplies were transported on an additional ion propelled ship.

18

As much as feasible, supplies were to be pre-launched from LEO towards Mars using ion propulsion. Fuel for the return journey along with provisions, the Mars surface habitat, and the Mars lander is sent to Mars on ion-engine propelled ships to save mass. Fuel for Mars Escape, Earth Return Injection, and Earth Capture is carried by two ion propelled tankers that take 5 years to reach Mars Orbit. Each tanker carries 632,000 kilograms of fuel and oxidizer, reactor and radiator to power the cryogenics system and the ion engines. The reactor and ion drive systems detach from the tankers and return on low energy orbits upon docking with the command ship.
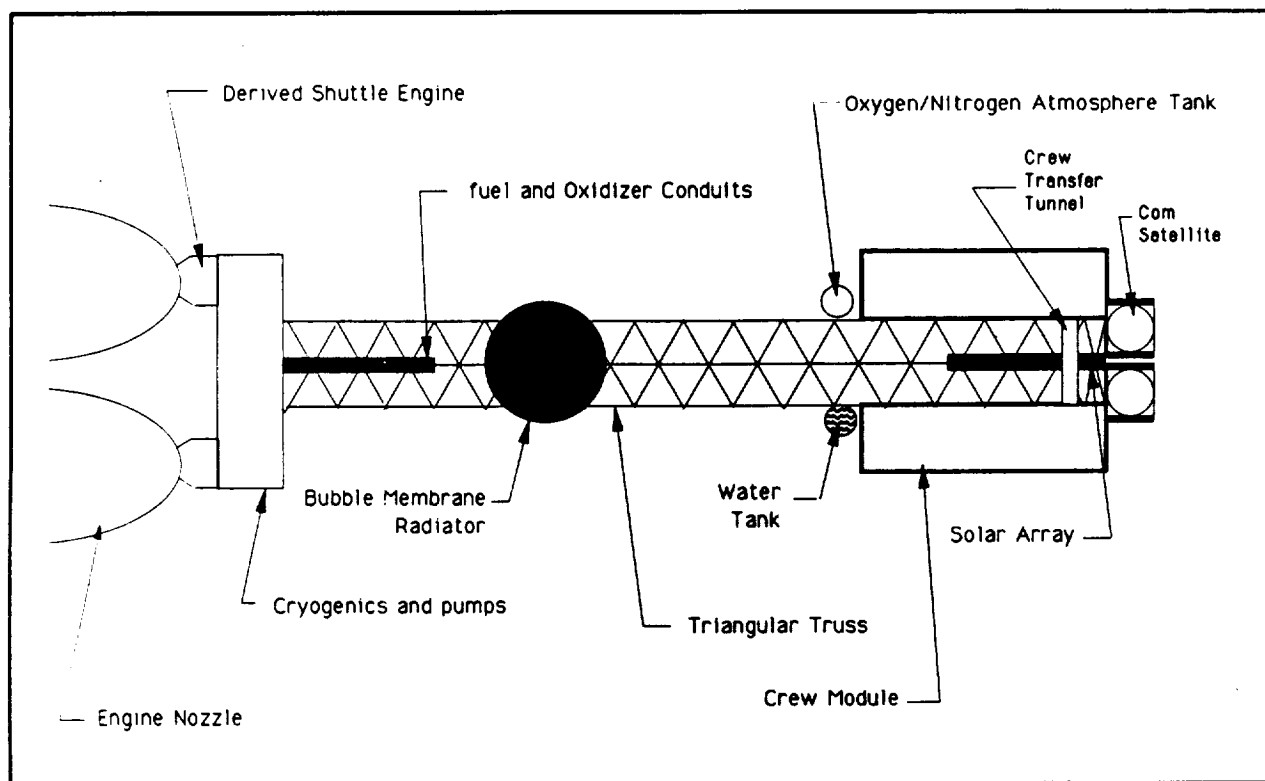
Figure 8: Command Ship

The command ship (Fig. 8) contains the following major components: the main engines, cryogenics and pumps, habitation module, laboratory module, solar array, wasteheat radiators, recycling system, storage tanks, and support structure.

The command ship relies on two engines derived from the space shuttle to provide all of the necessary thrust for the mission. These engines are derated space shuttle engines

that have the capability for multiple, long term burns at a greater I_{sp}. Nozzle extensions of ten meters diameter are used. They are divided into arc sections along the circumference. These sections are then latched together on orbit. The main engine, the converging section of the nozzle, the throat section, and a small section of the diverging section of the nozzle are carried as a unit into orbit in the shuttle bay. These engines provide a thrust of 60,000 Newtons each with an I_{sp} of 493 seconds.

The cryogenics and pumps that will maintain fuel, oxidizer, and breathing air supplies in the liquid state are similar to ground systems but will be optimized for space use. The optimization will include both volume and mass conservation.

The mass table for the command ship in LEO prior to Mars departure is as follows:

ITEM	MASS (KG)
Engines (2)	2,000.00
Comsats (2)	1,500.00
Survey Plane	204.70
Science Equipment	1705.70
Crew Clothing and Personal Effects	400.00
Food	636.00
Habitats Including Oxygen Scrubber	45,000.00
Water Supply	1,268.08
Air Supply	1635.30
Water Recycling Unit	182.00
Misc. Structural Mass	1768.22
Solar Array	250.00
Attitude Control Fuel	300.00
Docking Mechanism Mass	150.00
Aerobraking Mechanism	1,000.00
TOTAL	58,000.00

Table 6: Command Ship Mass Table

Ion propulsion is one of the most efficient propulsion systems currently available. The only drawback and the cause of its preclusion from manned missions is the low thrust associated. To achieve the fifty Newtons of thrust for each tanker, a cluster of twenty-five engines must be assembled.

Each tanker (Fig. 9) carries enough fuel aboard to execute a change in velocity of the fully loaded command ship of 11,980 m/s. Therefore, a single tanker in LEO is all that is required to escape Earth and capture at Mars. This assumes that the command ship is designed for an aerobraking change in velocity of approximately 3 km/s.

At Mars, the command ship will approach a second tanker in a 24 hour orbit about Mars. The tanker will then be commanded to separate from its reactor and ion engines. This unit will then commence a burn returning it to Earth and the command ship will dock with the second tanker. The second tanker will provide enough fuel and oxidizer to give the command ship, with its reduced mass, a ΔV of 12,530 m/s. This is more than enough to escape Mars and to enter the transfer ellipse.
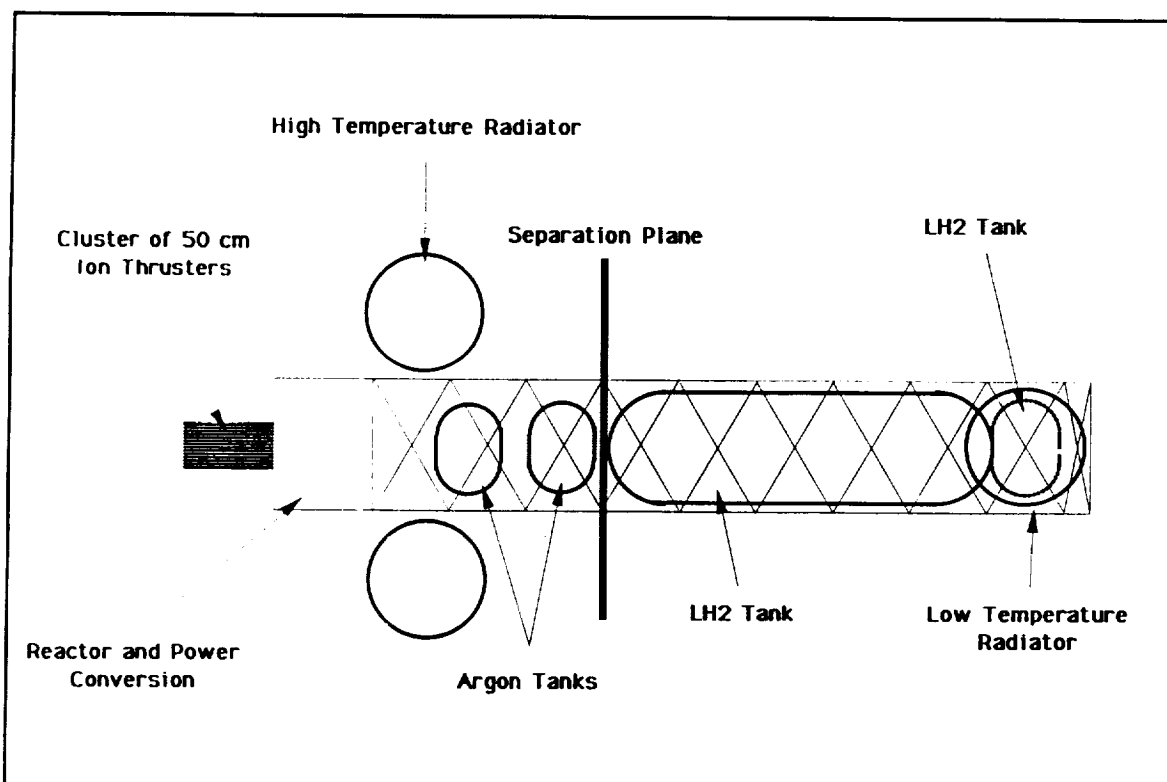
Figure 9: Tanker for Refueling Manned Ship

The last tanker will be along the transfer ellipse from Mars as stated in the mission overview. The reactor and engine assemblies will be separated and returned to Earth as stated previously. The remaining fuel from tanker 2 will be used to intercept tanker 3 and dock. Tanker 2 will then be jettisoned and the command ship will dock with tanker 3. Four bubble membrane radiators about 7.5 meters in diameter are used.

The tankers carry 380,000 kg of fuel and oxidizer. This figure was obtained from the propulsion analysis using the full mass of the command ship and the largest single ΔV requirements for a leg of the journey between refueling. The tankers also carry an additional 87,000 kg of liquid argon to fuel the ion thrusters.

The cargo ship is a tanker with the LOX and LH2 tanks removed. The Mars lander and surface habitat are substituted in their place.

5. REFERENCES

1. Buden, El-Genk, Lapin, et. al., "System Design Optimization for Multi-Megawatt Space Nuclear Power Applications," *Journal of Jet Propulsion*, Vol. 6, No. 3, March-April, 1990, pp. 194-202.

2. Hudson, S.L., "A Simplified Sizing and Mass Model for Axial Flow Turbines," *Proceedings of the 24th International Energy Conversion Engineering Conference, 1989*, Vol. 2, pp. 1091-1096.

3. Atwell, Salamah, Sinha, and Zarghami (GE Astro Space Division), "Thermoelectric Electro-Magnetic Pump Design for the SP-100 Reference Flight System," *Proceedings of the 24th International Energy Conversion Engineering Conference, 1989*, Vol 2, pp. 1227-1229.

4. Owen, Donald F., "SP-100/Brayton Power System Concepts," *Proceedings of the 24th International Energy Conversion Engineering Conference, 1989*, Vol. 2, pp. 1257-1261.

5. Begg, L.L. and Engdahl, E.H., "Advanced Radiator Concepts," *Proceedings of the 24th International Energy Conversion Engineering Conference, 1989*, Vol. 1, pp. 75-80.

6. Grossman, G. "Absorption Heat Pumps for Enhancement of Heat Rejection from Spacecraft," *Proceedings of the 24th International Energy Conversion Engineering Conference, 1989*, Vol. 1, pp. 51-56.

7. Agrawal, Brij N., *Design of Geosynchronous Spacecraft*, Prentice-Hall, 1986.

8. Antoniak, Z.I., and Webb, B.J., "Rotating Bubble Membrane Radiator for Space Applications," *Proceedings of the 21st International Energy Conversion Engineering Conference, 1986*, Vol. 3, pp. 1881-1885.

9. Klein, A.C., Pauley, K.A, and Webb, B.J., "Condensation Fluid Dynamics on Rotating Spherical Surfaces in a Microgravitational Field," *7th Symposium on Space Nuclear Power Systems*, Albuquerque, New Mexico, January 1990.

10. Apley, W.J. and Babb, A.L., "Thermal and Dynamic Analysis of the RING Power System Radiator," *6th Symposium on Space Nuclear Power Systems*, Albuquerque, New Mexico, January, 1989.

11. Koenig, D.R. "Rotating Film Radiators for Space Applications," *Proceedings of the 20th International Energy Conversion Engineering Conference, 1985*, Vol. 1, pp. 1,439-1,444.

12. Begg, L.L. and Wetch, J.R., "Comparison of High Temperature Heat Rejection Concepts to System-Related Requirements," *Proceedings of the 22nd International Energy Conversion Engineering Conference, 1987*, Vol. 1, pp. 227-234.

13. Brown, N. "Mars Transit Vehicle Thermal Protection System: Issues, Options, and Trade-offs," *Manned Mars Missions--Working Group Papers*, Vol. 2, Section 5, NASA, June 1986, pp. 745-755.

14. Comer, G., "Mars Vehicle Thermal Control System and Aerobrake Thermal Protection System," *Manned Mars Missions--Working Group Papers*, Vol. 2, Section 5, NASA, June 1986, pp 755-759.

15. Berkopec, F., Coomes, E.P., Cuta, J.M., et. al., "PEGASUS--A Multi-Megawatt Nuclear Electric Propulsion System," *Manned Mars Missions--Working Group Papers*, Vol. 2, Section 5, NASA, June 1986, pp. 769-786.

16. Dauro, V.A. "Aerobraking," *Manned Mars Missions--Working Group Papers*, Vol. 1, Section 1, NASA, June 1986, pp. 21-36.

17. Hill, O. and Wallace, R.O., "Manned Mars Mission Vehicle Design Requirements for Aerocapture," *Manned Mars Missions--Working Group Papers*, Vol. 1, Section 1, NASA, June 1986, pp. 114-128.

18. Braun, R.D., Hartung, L.C., and Powell, R.W., *Effect of Interplanetary Trajectory Options on a Manned Mars Aerobrake Configuration*, NASA Technical Paper 3019, August, 1990.

19. Determan, W.R. and Moriarty, M.P., "SP-100 Advanced Radiator Designs for Thermoelectric and Stirling Applications," *Proceedings of the 24th International Energy Conversion Engineering Conference, 1989*, Vol. 2, pp. 1245-1250.

20. Cess, R.D., and Sparrow, E.M., *Radiation Heat Transfer*, Hemisphere Publishing Corporation, Washington D.C., 1978.

21. Longuski, J.M. and Puig-Suari, J., *Hyperbolic Aerocapture and Elliptic Orbit Transfer with Tethers*, School of Aeronautics and Astronautics, Purdue University, 1991.

University of California, Los Angeles

Department of Mechanical, Aerospace, and Nuclear Engineering

GROUND SPEED OF BALLOONS ON MARS

ABSTRACT

In 1996 a joint Soviet, French, and American unmanned mission to Mars will be undertaken. Placed in the Martian atmosphere, scientifically instrumented balloons will carry below them a flexible, segmented guide rope or "snake." As the snake drags along the Martian surface, a variety of instruments will collect data. Key to the understanding of surface features and the atmosphere is the speed of the snake as it is dragged across the landscape. In the following report the design of a self-contained instrument which provides that measurement is discussed. Currently underway is the task of obtaining actual accelerometer data from a model snake for further evaluation.

1. INTRODUCTION

A topic of much scientific inquiry is the fourth planet, Mars. In order to study its surface more closely, an international space mission will be launched in 1996, lead by the Soviet Union with French and American cooperation. One of the cornerstones of this mission will be the deployment of the Soviet/French *Mars Balloon*, a wind driven balloon carrying a gondola and a guide rope or "snake" containing scientific instrumentation.

A principal function of the snake will be to compensate for the changing buoyancy of the balloon resulting from such changes as surface height, ambient pressure, balloon gas temperature and atmospheric and solar radiation (Fig. 1). In an effort to better understand the Martian surface features, the Planetary Society of the United States has proposed placing instrumentation in the snake itself. In addition to acquiring useful data concerning Mars, the performance of the balloon system can also be evaluated. The primary measurements include tether tension, snake geometric configuration, dynamic behavior, and surface speed.

In order to investigate the dynamic behavior of the snake/balloon unit, it is important to measure the tension at the junction between snake and balloon tether. As the snake

traverses the Martian landscape, the balloon tether may experience a range of tensions depending upon local conditions. For instance, when yielding materials such as sand are traversed, particularly large drag may be experienced.

Another principal parameter needed to describe the characteristics of the terrain as well as the state of snake/balloon unit, is the fraction of snake mass in contact with the surface. Measuring the angle made by the snake's nose, with the horizontal, known as the lean angle, will reveal the state of the balloon relative to the snake. Along with bending between segments and local accelerations, the roughness of the terrain can be identified.
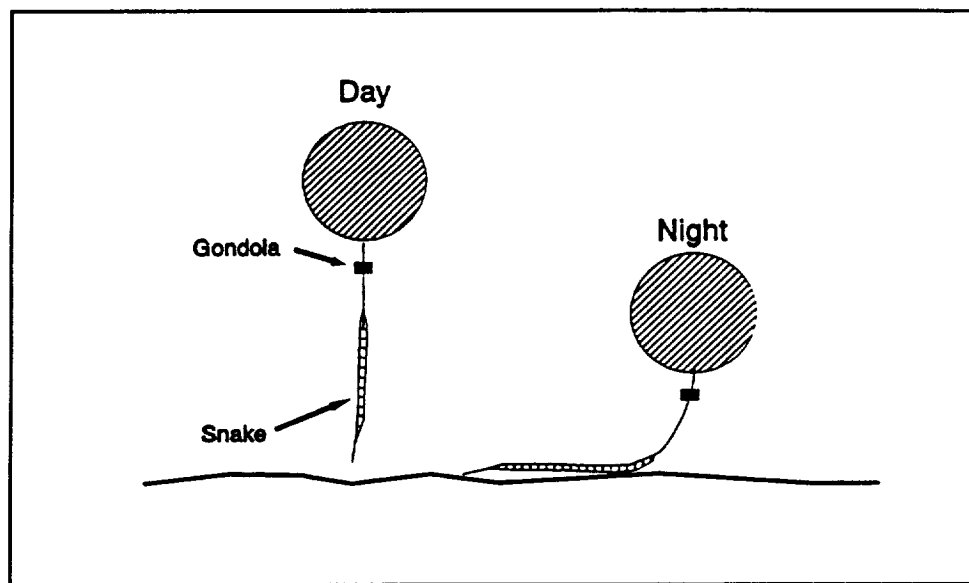
Figure 1: Daily Ballon Cycle as a Reaction to Buoyancy Changes

The designers have placed certain design constraints on the instrumentation to be used as a speedometer. The mechanism must not weigh more than 150 grams, including batteries and data processing equipment, and must not protrude from the skin of the snake so as not to snag on obstacles. Traveling over sandy and rocky surfaces, the snake will encounter considerable forces. The instrumentation in the snake must be capable of withstanding these shocks as well as other environmental factors.

Described here is the development of an accelerometer correlation speedometer, consisting of two pairs of orthoganally oriented accelerometers at different locations along

the snake (Fig. 2). As the snake moves along the surface, the accelerometers will respond to the surface features by producing an analog signal proportional to the magnitude of their acceleration in the plane perpendicular to the snake's direction of motion. As the snake encounters obstacles, a time delay will occur between the first and second set of accelerometers producing signals in reaction to the same obstacle. A convolution integral performed on the resulting signals will identify the lag time between them. By multiplying the inverse of this value by the distance between the pairs of accelerometers, the speed can be determined.

The following tasks were undertaken to accomplish the construction and testing of the correlation speedometer: A snake was designed to contain the two pairs of accelerometers for data gathering purposes. Computer software was developed to calculate the convolution integral and speed, first on artificially produced accelerometer data and eventually on data obtained from the model snake.

2. THEORY

The accelerometer pairs are spaced about two meters apart to insure that each pair experiences the same terrain features, but with a finite time delay τ between each of the two responses. This time delay corresponds to the amount of time it will take for the snake to move through a distance l equal to the separation between the two accelerometer pairs. Thus, if τ is known, the speed v of the snake can be calculated from the relation $v = l/\tau$.

The value of τ is obtained by the application of the convolution integral,

$$C(\tau) = \int a_1(t) a_2(t - \tau) dt \tag{1}$$

where $a_2(t)$ is the resultant of the accelerations of the leading accelerometer pair, and $a_1(t)$ the corresponding acceleration of the trailing accelerometer pair. If $a_1(t) = a_2(t - \tau)$, which will be the case if each accelerometer pair does indeed follow the same trail, then $C(\tau)$ in Eq. (1) will exhibit a maximum at $\tau = \tau^*$. In reality however, because of random noise in the accelerometer signals and because the paths of the two accelerometer pairs will deviate

slightly, $a_1(t)$ will not be precisely equal to $a_2(t - \tau)$, in which case the maximum $C(\tau^*)$ in Eq. (1) may not correspond to the correct τ. In this situation, it is better to use the centroid of $C(\tau)$. Both of these alternatives to the evaluation of τ were investigated in the computer simulations.
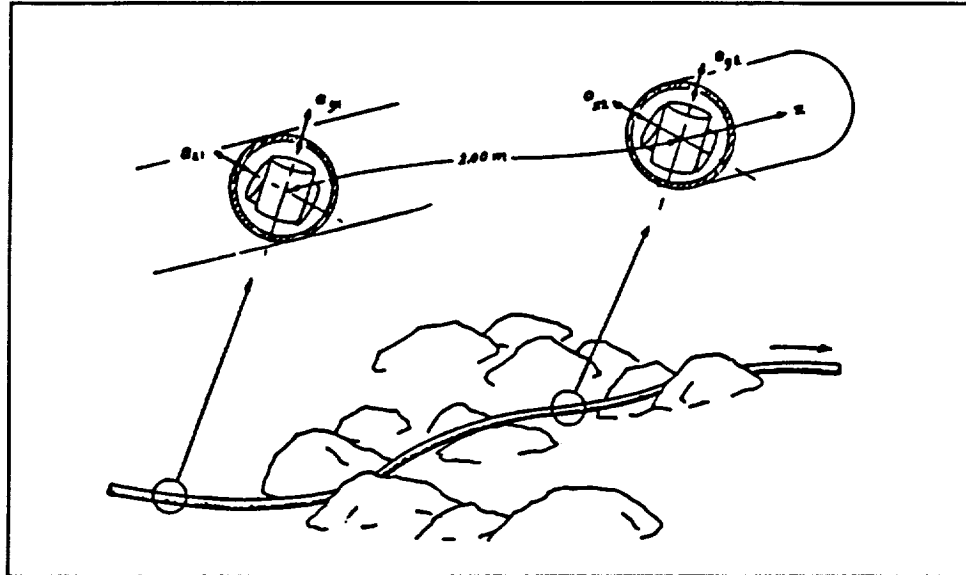
Figure 2: Accelerometer Orientation and Location Along Snake

3. SOFTWARE TERRAIN SIMULATION

The computer simulations consisted of generating simulated accelerometer response data from a given ground profile and snake velocity, calculating $C(\tau)$ from Eq. (1) and plotting it versus τ associated with the maximum and the centroid and comparing the corresponding snake speeds with the originally assumed value. The ground profile used in the first stage of the simulations was a simple two dimensional "rock," represented by a Guassian normal distribution,

$$z(x) = z_0 \exp[-(x/x_0)^2] \tag{2}$$

4

where z_0 and x_0 are arbitrary constants. Of course, the rocks on Mars are not shaped like normal distributions, but for the purpose of validating the analysis program, the Gaussian is ideally suited because of its mathematical simplicity and because it does not have any discontinuities which would lead to singularities upon differentiation. This is probably a reasonably realistic situation since any discontinuities in the motion of the accelerometers arising from discontinuities on the surface are likely to be smoothed out by the limited flexibility of the snake.

Because the simulations were limited to two dimensions, response data was simulated for only two accelerations, each sensitive to acceleration in the vertical direction. The accelerations to be analyzed were calculated by differentiating the vertical displacements. Differentiating Eq. (2) twice gives,

$$a(x) = \frac{d^2 z(x)}{dx^2} = \frac{-2z_0}{x_0^2} \left[\exp - (x/x_0)^2 \right] \left[1 - \frac{2x^2}{x_0^2} \right] \tag{3}$$

and

$$a(t) = \frac{d}{dt} \left[\frac{dz}{dx} \right] \left[\frac{dx}{dt} \right] = \left[\frac{d^2 z}{dx^2} \right] \left[\frac{dx}{dt} \right]^2 \tag{4}$$

But dx/dt in Eq. (4) is simply the velocity v of the snake, so combining equations (3) and (4) gives,

$$a(t) = v^2 \frac{d^2 z}{dx^2} = -2z_0 \frac{v^2}{x^2} \left[\exp -(x/x_0)^2 \right] \left[1 - \frac{2x^2}{x_0^2} \right] \tag{5}$$

The random noise fluctuations which will undoubtedly be present in the accelerometer signals were modelled by a function of the form,

$$a_r(t) = v^2 z_0 / x_0^2 \, \epsilon \phi(x) \tag{6}$$

5

where $\phi(x)$ is a random function which takes on values from -1 to 1, and ϵ is a variable parameter which represents the magnitude of the random fluctuations relative to the actual accelerations induced by the surface. The sensitivity of the speed calculations to the magnitude of the random fluctuations could then be investigated by varying the value of ϵ for different simulation runs. With

$$x_1 = vt - l/2, \quad x_2 = vt + l/2 \tag{7}$$

and

$$\alpha_1(t) = \frac{l}{x_0}(t/\tau + 1/2), \quad \alpha_2(t) = \frac{l}{x_0}(t/\tau - 1/2) \tag{8}$$

Expressions for the total output signals of each accelerometer pair are then given by combining equations (5) and (6), and using identities (7) and (8) to write them explicitly as functions of time,

$$a_i(t) = \frac{l^2 v^2}{\tau^2 x_0^2}\left\{2e^{-\alpha_i^2(t)}(2\alpha_i^2(t) - 1) + \epsilon\phi_i(t)\right\}, \quad i = 1,2 \tag{9}$$

Additionally, the ground profile for the simulations was expanded to accommodate several rocks randomly distributed along the surface.

4. CORRELATION SOFTWARE

A computer program was written in Fortran to perform an analysis of the data produced by the algorithm described above. Accelerations were read in as discrete values in time separated by a chosen interval, Δt. The program analyzes the data using the convolution integral of Eq. (1), represented in discrete form by,

$$C(n) = \sum \alpha_{1,j} a_{2,j-n}\Delta t \tag{10}$$

where the subscript j represents increments of time and n is the number of time increments in τ. The range of n used in Eq. (11) is supplied by the user as input for each run. The program searches for n_{max} and calculates the centroid of $C(n)$ by the relationship,

$$n_{ct} = \frac{\displaystyle\sum_{n-n_{start}}^{n_{end}} n|C(n)|}{\displaystyle\sum_{n-n_{start}}^{n_{end}} |C(n)|} \tag{11}$$

The corresponding estimates of the snake's speed are then calculated from,

$$V_{max} = \frac{l}{\tau_{max}} = \frac{l}{n_{max}\Delta t} \tag{12}$$

$$V_{ct} = \frac{l}{\tau_{ct}} = \frac{l}{n_{ct}\Delta t} \tag{13}$$

5. SIMULATION RESULTS

The values of various parameters used in calculating the simulated environment were:

l = 2 m

V = 10 m/sec

$z_0 = x_0 = 0.5$ m

Δt = 0.01 sec

The first simulation that was run was for the ground profile given by Eq. (2) with no random fluctuations in the accelerometer signals (Fig. 3). For this simple case, a distinct maximum occurred at $n = 20$ which is identified correctly. As might be expected, however, the calculation of the centroid is strongly dependent on the range of n selected. In order for the program to correctly identify the centroid, the range of n considered in Eq. (11) must be large enough to encompass a sufficient range of values on either side of the correct one. In general, the correct value will not be known beforehand, thus the range of n used in the

7

analysis must be wide enough to encompass all possible values. Because the snake is not likely to be moving backwards, an appropriate lower limit for this range is $n_{start} = 0$ (which would correspond to an infinite snake speed). The upper limit will depend on the selected value of Δt and on the smallest speed of interest, $n_{end} >> l/\Delta t V_{min}$.
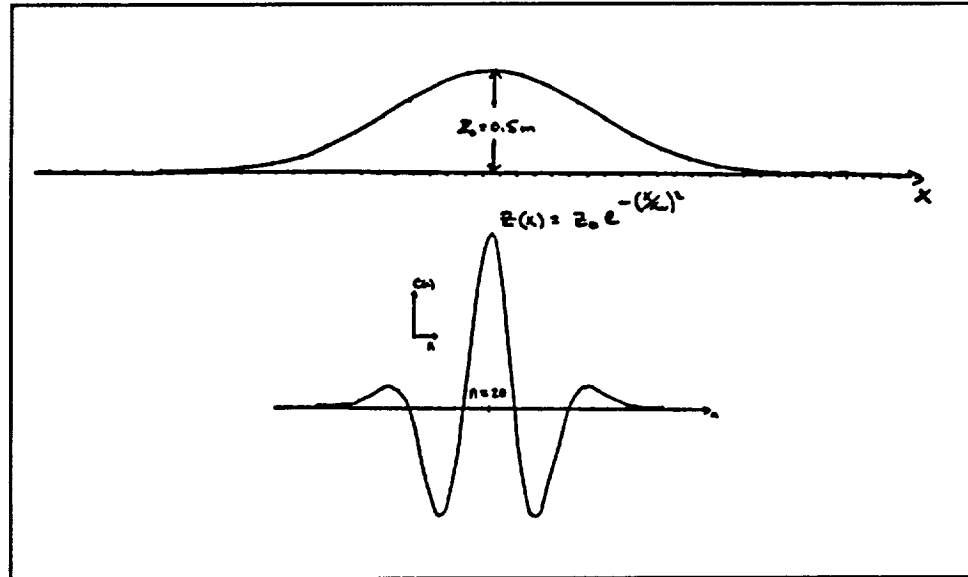
Figure 3: Simple (Gaussian) Rock Profile and Convolution Integral

The next stage in the simulations was to introduce random fluctuations into the accelerometer outputs. To begin, an ϵ value of 1.0 was introduced. In this case, a strong n_{max} occurred at $n = 13$ rather than $n = 20$, causing an error of 54% in the calculated speed. The centroid however occurred at $n = 19$, much closer to the correct value of $n = 20$, and provided a speed estimate within 5% of the actual speed. Other values of ϵ were introduced and it was determined that the erroneous n_{max} values occurred when ϵ exceeded 0.8, while the centroid value remained reasonably consistent.

Finally, the correlation was performed on a set of signals representing terrain with multiple rocks. Random noise fluctuations in the multiple rock environment produced erroneous n_{max} values when ϵ exceeded 0.6. But a different phenomenon affected the centroid of $C(n)$ when multiple rocks with identical shapes were used. With no random

8

fluctuations in the data, the centroid of $C(n)$ occurred at $n = 14$, and V_{ct} was erroneous by 43%. It can be deduced that the centroid of $C(n)$ depends not only on the random fluctuations in the data and the range of n considered, but also on the distribution of rocks in the sample space.

Overall, the result of the simulations look very encouraging. In essence, they indicate that the speed of the snake can be calculated with a high degree of reliability as long as the magnitude of the random fluctuations in the accelerometer readings is not more than about 3/8 of the total. These random fluctuations can be due to a variety of sources, such as vibrations in the snake, electronic noise in the signals, or even differences in the paths of the two accelerometer sets. Thus, more testing will have to be done before the actual magnitude of these fluctuations will be known. If their magnitude is indeed greater than 3/8 of the total, a way will have to found to lessen their effect on the speed calculations. Possible solutions to this problem include filtering the accelerometer signals and removing secondary maxima in $C(n)$. The error associated with a field of multiple rocks was most likely caused by the fact that each "rock" had an identical shape. This should be alleviated by the large variation of surface obstacles encountered on actual terrain.

5. DESIGN OF MODEL MARS SNAKE

In order to test the speedometer, a satisfactory model of the actual snake had to be designed and constructed. The snake that is being currently tested for use on Mars is segmented, and consists of individual shells linked by a steel cable running down their center.

It was decided that for our tests it was not feasible or necessary to construct a complex snake just to gather data. In place of the original design, a scaled down model was designed to more closely meet the requirements of the data gathering. It consisted of three two meter long pieces of flexible thin walled tubing. The three segments were joined by circular clamps to two four inch pieces of aluminum tubing. The nose and tail of the snake were capped with aluminum cones, and trailing the tail was a piece of steel cable which keeps the rear of the snake from whipping when it is dragged. The accelerometers were sealed in rubber molds to simplify mounting. Each set was housed in one of the two

9

aluminum tubes. Coaxial cables linked each accelerometer with an electrical connection at the nose of the snake.
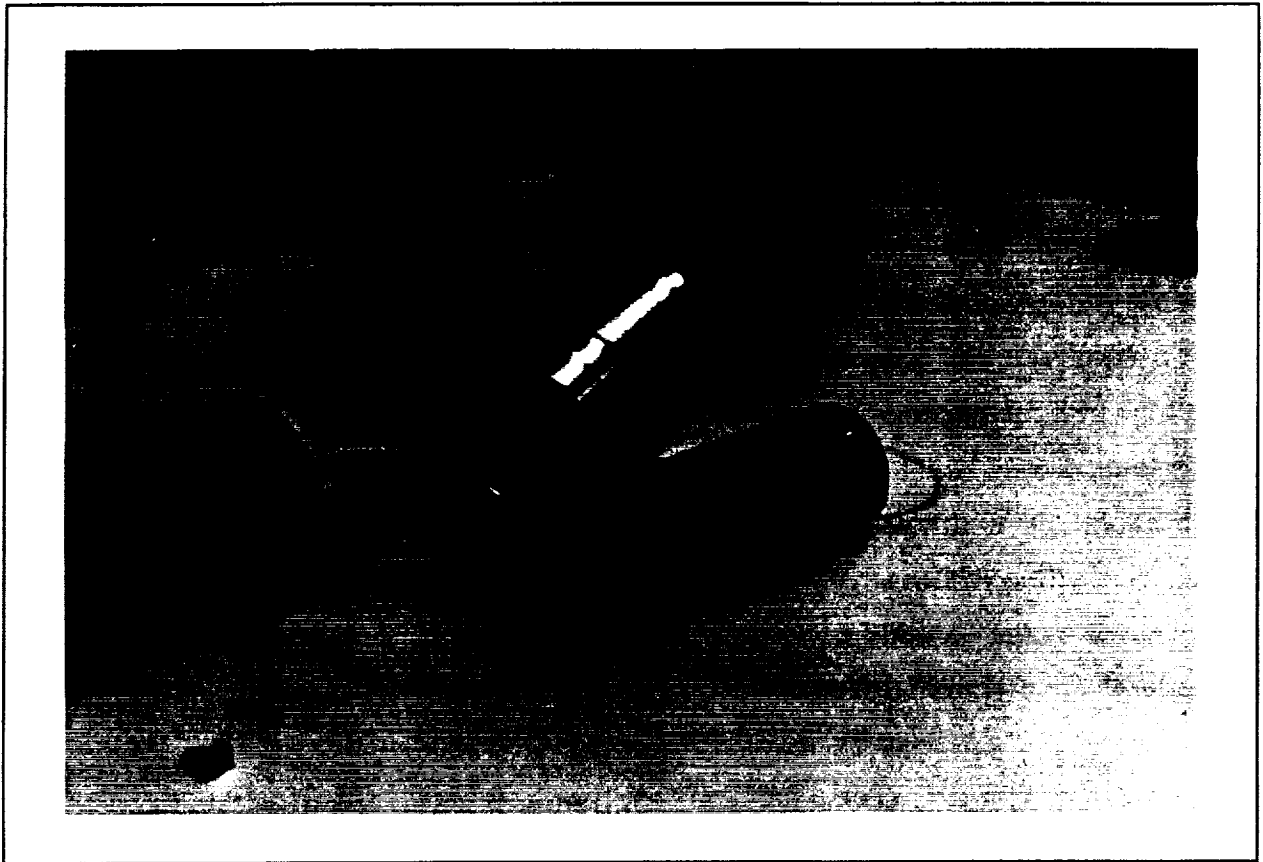
Figure 4: Accelerometers Embedded in RTV Compound

At this time the model snake has been constructed and the support equipment needed to obtain data is being gathered. An IBM XT computer and analog-to-digital data acquisition board will be used to store accelerometer data. A first field test on the UCLA campus was conducted with good results.